eNeuro

Research Article: New Research | Neuronal Excitability

High-Precision Fast-Spiking Basket Cell Discharges during Complex Events in the Human Neocortex

Human basket cell firing in complex events

Viktor Szegedi[1], Gábor Molnár[2], Melinda Paizs[1], Eszter Csakvari[1], Pál Barzó[3], Gábor Tamás[2] and Karri Lamsa[1]

[1]MTA-NAP Research Group for Inhibitory Interneurons and Plasticity, Department of Physiology, Anatomy and Neuroscience, University of Szeged, Közép Fasor 52, Szeged, 6726, Hungary

[2]MTA-SZTE Research Group for Cortical Microcircuits, Department of Physiology, Anatomy and Neuroscience, University of Szeged, Közép Fasor 52, Szeged, 6726, Hungary

[3]Department of Neurosurgery, University of Szeged, Semmelweis u. 6, Szeged, 6726, Hungary

DOI: 10.1523/ENEURO.0260-17.2017

Received: 25 July 2017

Revised: 7 September 2017

Accepted: 11 September 2017

Published: 27 September 2017

Author contributions: V.S., G.M., G.T., and K.P.L. designed research; V.S., G.M., M.P., E.C., and K.P.L. performed research; V.S., G.M., M.P., E.C., P.B., and K.P.L. analyzed data; P.B. and G.T. contributed unpublished reagents/analytic tools; K.P.L. wrote the paper.

Funding: National Brain Research Program
KTIA_NAP_13-2-2015-0005

Funding: ERC INTERIMPACT

Funding: Hungarian Academy of Sciences

The authors declare no competing financial interests.

This work was supported by National Brain Research (Nemzeti Agykutatási) program (KL, MP, VS, EC, GM and GT), the ERC INTERIMPACT project (GT), and the Hungarian Academy of Sciences (GM, GT and VS). We acknowledge Márton Rózsa, Drs Szabolcs Oláh and János Szabadics for some recordings included in this study, Nelli Ábrahám-Tóth for help with cell reconstructions, and Dr Gareth Morris for their comments on the manuscript.

V.S. and G.M. contributed equally to this work.

Correspondence should be addressed to either Gábor Tamás, email: gtamas@bio.u-szeged.hu or Karri Lämsä, email: klamsa@bio.u-szeged.hu

Cite as: eNeuro 2017; 10.1523/ENEURO.0260-17.2017

High-precision fast-spiking basket cell discharges during complex events in the human neocortex

Abbreviated title: *Human basket cell firing in complex events*

Viktor Szegedi[1¶], Gábor Molnár[2¶], Melinda Paizs[1], Eszter Csakvari[1], Pál Barzó[3], Gábor Tamás[2*] and Karri Lamsa[1*]

[1]*MTA-NAP Research Group for Inhibitory Interneurons and Plasticity, Department of Physiology, Anatomy and Neuroscience, University of Szeged, Közép fasor 52. Szeged, 6726 Hungary*

[2]*MTA-SZTE Research Group for Cortical Microcircuits, Department of Physiology, Anatomy and Neuroscience, University of Szeged, Közép fasor 52. Szeged, 6726 Hungary*

[3]*Department of Neurosurgery, University of Szeged, Semmelweis u. 6. Szeged, 6725 Hungary*

¶ These authors contributed equally to this work.

* Correspondence to: Gábor Tamás, email: gtamas@bio.u-szeged.hu and Karri Lämsä, email: klamsa@bio.u-szeged.hu

Number of pages: 32

Number of figures : 4

Number of words in abstract (231), introduction (425), discussion (897)

The authors declare no competing financial interests

Acknowledgements: This work was supported by National Brain Research (Nemzeti Agykutatási) program (KL, MP, VS, EC, GM and GT), the ERC INTERIMPACT project (GT), and the Hungarian Academy of Sciences (GM, GT and VS). We acknowledge Márton Rózsa, Drs Szabolcs Oláh and János Szabadics for some recordings included in this study, Nelli Ábrahám-Tóth for help with cell reconstructions, and Dr Gareth Morris for their comments on the manuscript.

ABSTRACT

In the human neocortex, solitary action potentials in some layer 2-3 pyramidal cells (PCs) trigger brief episodes of network activity known as complex events through strong excitatory synapses that specifically innervate GABAergic interneurons. Yet, how these ”master PCs” configure the local network activity is not well understood. We report that single spikes in the PCs, studied here in synaptically connected cell pairs in frontal or temporal neocortical areas of both males and females, elicit firing of fast-spiking basket cells (FSBCs) with a short delay (on average 2.7 ms). The FSBC discharge is triggered by 13 mV (on average) monosynaptic excitatory postsynaptic potentials, and the action potential is time-locked to the master PC spike with high temporal precision, showing little jitter in delay. In the complex events, the FSBC discharge occurs in the beginning of the activity episode, forming the first wave of the complex event activity. Firing of FSBCs generates GABAergic inhibitory postsynaptic currents (IPSCs) with fast kinetics in layer 2-3 PCs, and similar IPSCs regularly occur time-locked to master PC spikes in the beginning of the complex events with high probability and short (median 4.1 ms) delay with little jitter. In comparison, discharge of non-fast spiking interneurons investigated here appears inconsistently in the complex events and shows low probability. Thus, firing of layer 2-3 FSBCs with high temporal fidelity characterizes early phase of the complex events in the human neocortex.

SIGNIFICANCE STATEMENT

In the human neocortex solitary action potentials of some pyramidal cells (PCs) trigger network activity episodes known as complex events. These ”master PCs” with

53 remarkably strong synapses occur widely in the human neocortical layers 2 and 3, but
54 are not found in rodent neocortex and little is known about the network activity they
55 evoke. We report that the master PCs configure neocortical network activity in a precise
56 manner by activating specialized inhibitory interneurons, fast-spiking basket cells
57 (FSBCs), in the beginning of the complex events with an accurate temporal pattern.
58 Temporally patterned high-precision firing of FSBCs is a hallmark of many physiological
59 processes in the neocortex, and our results show that solitary PC spikes can initiate such
60 activity in humans.

61

62 INTRODUCTION

63 Information in the neocortex is encoded by the temporally organized discharge of
64 neuronal ensembles, and this requires timed activation of specialized GABAergic
65 interneurons (Ainsworth et al., 2012; Buzsaki and Watson, 2012). Human neocortical
66 microcircuits show a low threshold for generation of small-scale neuronal population
67 activity, because strong multivesicular excitatory synapses connect some layer 2-3
68 pyramidal cells (PCs) to GABAergic interneurons with very large suprathreshold
69 postsynaptic excitatory potentials (VLEs). Consequently, a solitary spike in the ”master
70 PC” triggers firing in the local interneurons, initiating a tens-of-milliseconds -long
71 population burst known as a complex event (Molnar et al., 2008; Brecht, 2012; Molnar
72 et al., 2016; Szegedi et al., 2016). Although the complex events occur in various
73 neocortical areas in humans, similar solitary PC spike -evoked network activity episodes
74 have not been reported in the rodent neocortex (Molnar et al., 2008; Komlosi et al.,
75 2012; Doron and Brecht, 2015; Molnar et al., 2016; Szegedi et al., 2016; Lourenco and
76 Bacci, 2017). A specific role of the complex events in the human neocortical

77 microcircuits is unknown, but it has been proposed that master PCs may have evolved
78 in the evolutionary process to support generation of neuronal ensembles in higher-
79 order cerebral functions (Komlosi et al., 2012; Lourenco and Bacci, 2017). If this
80 hypothesis is correct, one would also expect the complex events to exhibit temporal
81 patterns in discharge of the neurons, as temporally structured firing characterizes
82 neuronal ensembles (Isaacson and Scanziani, 2011; Brecht, 2012; Buzsaki and Watson,
83 2012). Hence, we investigate here whether the master PC-evoked complex events show
84 temporally organized discharge of a specific GABAergic interneuron type, the fast-
85 spiking basket cell (FSBC). The FSBCs have a well-established role in generation of co-
86 ordinated cortical high-frequency network activities involved in cognitive processes
87 and they are key players in the neuronal ensemble activity (Buzsaki and Watson, 2012;
88 Lewis et al., 2012), The experiments are carried out in slices from neocortical tissue
89 resected in surgeries for the operation of subcortical or deep cortical targets. First, we
90 investigate the FSBC firing delay and the action potential temporal precision elicited by
91 solitary master PC spikes. Second, we examine GABAergic output from the FSBCs and
92 some non-fast-spiking interneurons (non-FSINs) during master PC -evoked complex
93 events using dual recordings from pyramidal cells. The results show that master PC
94 spikes evoke high-precision firing of the FSBCs, and that the FSBCs are activated in the
95 first wave of GABAergic activity in the complex events. We conclude that the short-delay
96 discharge of FSBCs with high temporal precision is a regular feature of master PC-
97 evoked complex events in the human neocortex.

98

99 METHODS

Ethics Statement. All procedures were performed according to the Declaration of Helsinki with the approval of the University of Szeged Ethical Committee and Regional Human Investigation Review Board (ref. 75/2014). None of the experiments were reported before with a minor exception that in five of the fifteen cells reporting monosynaptic IPSCs in the figure 4A, one data parameter (IPSC amplitude) has been included in a previous manuscript (Szegedi et al. 2016). However, the other data parameters of these cells reported here (rise slope, normalized slope) have not been reported before.

Brain slices. Human neocortical slices were derived from material that had to be removed to gain access for the surgical treatment of deep-brain targets (tumour, cyst, aneurysm or catheter implant) from the left and right frontal, temporal, and parietal regions, with written informed consent of the patients prior to surgery. In some cases tissue from neocortical operations was used when it was non-pathological. In these latter cases, small pieces of non-pathological tissue had to be removed in the surgery to get access to pathological targets in the folded neocortex. The patients were 10–60 years of age, including 21 and 18 samples from males and females, respectively. The tissue obtained from underage patients was provided with agreement from a parent or guardian. Details including the patient gender, age, the resected neocortical area and the pathological target diagnosis are reported for all tissue samples used in this study in **Table 1**. Anesthesia was induced with intravenous midazolam and fentanyl (0.03 mg/kg, 1–2 lg/kg, respectively). A bolus dose of propofol (1–2 mg/kg) was administered intravenously. The patients received 0.5 mg/kg rocuronium to facilitate endotracheal intubation. The trachea was intubated and the patient was ventilated with O_2/N_2O mixture at a ratio of 1:2. Anesthesia was maintained with sevoflurane at care

volume of 1.2–1.5. Following surgical removal, the resected tissue blocks were immediately immersed into a glass container filled with ice-cold solution in the operating theatre. The solution contained (in mM): 130 NaCl, 3.5 KCl, 1 NaH_2PO_4, 24 $NaHCO_3$, 1 $CaCl_2$, 3 $MgSO_4$, 10 D(+)-glucose, and was saturated with 95 % O_2/5 % CO_2. The container was placed on ice in a thermally isolated transportation box where the liquid was continuously gassed with 95 % O_2/5 % CO_2. Then, the tissue was transported from the operating theatre to the electrophysiology lab (door-to-door in maximum 20 minutes), where slices of 350 µm thickness were immediately prepared from the block with a vibrating blade microtome (Microm HM 650 V). The slices were incubated at room temperature (22-24 °C) for 1 hour, when the slicing solution was gradually replaced by a pump (6 ml/min) with the solution used for storage (180 ml, content identical to a solution used in electrophysiology experiments). The storage solution was identical to the slicing solution, except containing 3 mM $CaCl_2$ and 1.5 mM $MgSO_4$.

Electrophysiology. Recordings were performed in a submerged chamber (perfused 8 ml/min) at 36–37°C. Cells were patched using water-immersion 20x objective with additional zoom (up to 4x) and infrared differential interference contrast video microscopy. In line with previous studies, VLEs were found in 10 - 15 % of PC to interneuron connections tested (Molnar et al., 2008; Szegedi et al., 2016). Spike transmission data were obtained 10 - 30 min after break-in to whole cell. Micropipettes (5–8 MΩ) for whole-cell patch-clamp recording were filled with intracellular solution (in mM): 126 K-gluconate, 4 KCl, 4 ATP-Mg, 0.3 Na_2–GTP, 10 HEPES, 10 phosphocreatine (pH 7.20; 300 mOsm) with 0.3 % (w/v) biocytin. Current- and voltage-clamp recordings were performed with a Mutliclamp 2B amplifier (Axon Instruments) or EPC 10 quadro amplifier (HEKA), and low-pass filtered at 6-8 kHz (Bessel filter).

Series resistance (Rs) and pipette capacitance were compensated in current clamp mode and pipette capacitance in the voltage clamp mode. Rs was monitored and recorded continuously during the experiments. Voltage clamp recordings were discarded if the Rs was higher than 25 MΩ or changed by more than 20 %. Spikes were generated in the presynaptic cell with brief (2–3 ms) suprathreshold depolarizing pulses in voltage clamp or current clamp mode (delivered every 10 s). Liquid junction potential error was corrected in all membrane potential values. Postsynaptic FSBC membrane potential in the experiments shown in figure 1 was moderately depolarized (3.4 ± 1.7 mV, FSBC 1-4) or hyperpolarized (-5.2 mV, FSBC 5) from the resting membrane potential (-63.8 ± 3.6 mV, n = 5) recorded immediately after break-in to whole cell, aiming to adjust VLE-evoked spiking probability between the half-maximum and maximum in the cells. Accordingly, the non-FSINs were depolarized 11.6 ± 7.3 mV from the resting membrane potential (-68.7 ± 2.2 mV) (n = 3). Membrane time constant and cell input resistance were measured in current clamp using -20 pA, 600-800 ms steps delivered at resting membrane potential. Firing frequency accommodation was tested by applying 600 - 800 ms depolarizing current steps to evoke firing between 30 and 40 Hz during the first 100 ms of the step. The non-FSIN 3 fired only single action potentials in response to the depolarizing steps, tested up to -20 mV.

Data Analysis and Statistics. Data were acquired with Clampex (Axon Instruments) or with PatchMaster software (HEKA) and digitized at 20–100 kHz. The data for EPSPs, IPSPs/Cs, action potential timing, axon current width, and the cell membrane time constant were analyzed off-line with p-Clamp (Axon Instruments, RRID: SCR_011323), Spike2 (version 8.1, Cambridge Electronic Design, RRID: SCR_000903), OriginPro (OriginLab Corporation, RRID: SCR_00281) and IgorPro (WaveMetrics Inc.,

RRID:SCR_000325) and SigmaPlot (RRID: SCR_003210) softwares. Data are presented as mean ± s.e.m, and for data with non-parametric distribution as median with lower and upper quartiles (interquartile range). For cell groups the data are calculated from the means of individual experiments (mean of means). Monosynaptic IPSCs, and di- and multisynaptic IPSCs were filtered off-line using RC low-pass with cut-off frequency corresponding to 80 microsecond tau. The VLE average amplitude values were calculated for each cell from the VLEs that failed to spike in the experiments. In the experiments where spiking probability was high, additional VLEs were measured in a subthreshold potential to yield at least 3 VLEs for each cell to calculate the mean. For dV/dt analyses of monosynaptic VLEs, a 0.12 ms sliding average window was used to measure trace derivatives. The maximum VLE rising slope was measured from the derivative by averaging data points within 0.3 ms of positive peak. Postsynaptic action potential onset in VLE-spike complexes was identified utilizing the response derivative, and membrane potential at this time point was used to define the firing threshold shown in figures 1 and 2. Evoked action potential delay to the presynaptic spike was calculated as a temporal distance of the pre- and postsynaptic spike peak. Spike kinetics in the interneurons were measured as the axon potential depolarizing phase width at half-maximal amplitude (in current clamp experiments), and as axon inward current width (in voltage clamp experiments).

VLE amplitude and time-to-peak, IPSPs and monosynaptic IPSCs were analyzed as described previously (Szegedi et al., 2016). For the IPSCs, derivative analysis was utilized to help to define the IPSC onset and the peak of individual IPSCs in the complex events as illustrated in figure panel 4*B2-3*. Rather than measuring the maximal rise slope directly from the IPSC derivative (because of small signal amplitude compared the

noise in the slow IPSCs), the IPSCs were confirmed by visual inspection and fitted with slope curve for rise slope (20-80%) analysis. The IPSC rise slope was divided by the IPSC amplitude to define the amplitude-normalized rise kinetics. In the experiments measuring the monosynaptic IPSCs (amplitude-) normalized rise slope values, the rise slope value inversely correlated with the IPSC amplitude, suggesting that the variation observed in the normalized slope values in individual cells possibly emerged from asynchrony of released vesicle quanta ($r = -0.73$, $P = 0.0000002$, $n = 60$ IPSCs in 6 FSBCs, Spearman Rank order correlation) (Mody et al., 1994). For statistical analysis, Anova on ranks with Dunn's multiple paired comparison (*post hoc* test), Mann-Whitney U-test (MW test) and t-test were used. Differences were accepted as significant if $P < 0.05$. Parametric distribution was tested with Shapiro-Wilk test using SigmaPlot (RRID: SCR_003210).

Cell Visualization and reconstruction. After electrophysiological recording, slices were immediately fixed in a fixative containing 4 % paraformaldehyde and 15% picric acid in 0.1 M phosphate buffer (PB, pH = 7.4) at 4° C for at least 12 h, then stored at 4 °C in 0.1 M PB with 0.05 % sodium azide as a preservative. Slices were embedded in 10 % gelatin and further sectioned into slices of 50 µm thickness in the cold PB using a vibratome VT1000S (Leica Microsystems). After sectioning, the slices were rinsed in 0.1 M PB (3 x 10 min) and cryoprotected in 10 – 20 % sucrose solution in 0.1 M PB. Finally, they were incubated in fluorophore (Cy3)-conjugated streptavidin (1:400, Jackson ImmunoResearch Lab.Inc.) in 0.1 M Tris-buffered saline (TBS, pH 7.4) for 2.5 h (at 22–24°C). After washing with 0.1 M PB (3 x 10 min), the sections were covered in Vectashield mounting medium (Vector Laboratories Inc.), put under cover slips, and examined under an epifluorescence microscope (Leica DM 5000 B). Sections selected

for immunohistochemistry and cell reconstruction were dismounted and processed as explained below in the *Immunohistochemistry* -paragraph. Some sections for cell structure illustrations were further incubated in a solution of conjugated avidin-biotin horseradish peroxidase (ABC; 1:300; Vector Labs) in Tris-buffered saline (TBS, pH = 7.4) at 4° C overnight. The enzyme reaction was revealed by the glucose oxidase-DAB-nickel method using 3'3-diaminobenzidine tetrahydrochloride (0.05 %) as chromogen and 0.01 % H_2O_2 as oxidant. Sections were further treated with 1 % OsO_4 in 0.1M PB. After several washes in distilled water, sections were stained in 1 % uranyl acetate and dehydrated in ascending series of ethanol concentration. Sections were infiltrated with epoxy resin (Durcupan) overnight and embedded on glass slides. For the cells visualized in the figures, three-dimensional light microscopic reconstructions from one or two sections were carried out using the Neurolucida system (RRID:SCR_001775) with 100x objective (Olympus BX51, Olympus UPlanFI). Images were collapsed in the z-axis for illustration. FSINs in figure panel 4*A2* referred to as unidentified FSINs (uFS) were unsuccessfully recovered for anatomical analysis.

Immunohistochemistry. Free-floating sections were washed 3 times in TBS-TX 0.3 % (15 min) at 22–24°C, then moved in 20 % blocking solution with horse serum in TBS-TX, 0.3 % for parvalbumin (pv) staining and 10 % blocking solution for vesicular GABA transporter (vgat) staining. The sections were incubated in primary antibodies diluted in 1 % serum in TBS-TX 0.3 % over three nights at 4° C, then put in relevant fluorochrome-conjugated secondary antibodies in 1 % of blocking serum in TBS-TX 0.3 % overnight at 4° C. Sections were washed at first step in TBS-TX 0.3 % (3 x 20 min) and later in 0.1 M PB (3 x 20 min) and mounted on glass slides with Vectashield mounting medium (Vector Lab.Inc.). The characterizations of antibodies: pv (goat anti-pv, 1:500,

Swant, Switzerland, www.swant.com, AB_10000343) and vgat (rabbit anti-vgat, 1:500, Synaptic Systems, Germany, www.sysy.com, AB_887871). Fluorophore-labelled secondary antibodies were: DyLight 488 (Donkey anti goat, 1:400, Jackson ImmunoResearch Lab. Inc., www.jacksonimmuno.com), Alexa488 (Donkey anti rat, 1:400, Jackson ImmunoResearch Lab. Inc.) and Cy5 (Donkey anti rabbit, 1:500, Jackson ImmunoResearch Lab. Inc.). Labelling of neurons by biocytin and immunoreactions were evaluated using first epifluorescence (Leica DM 5000 B) and then laser scanning confocal microscopy (Zeiss LSM880). The micrographs presented are confocal fluorescence images.

RESULTS

Single pyramidal cell spikes trigger fast-spiking basket cell discharges with short delay and high temporal precision through Very Large EPSPs

First, we studied firing of fast-spiking basket cells (FSBCs) evoked by single spikes in layer 2-3 master PCs. We recorded synaptically connected PC to FSBC pairs in whole-cell clamp to find master PCs generating Very Large EPSPs (VLE, average amplitude 13.4 ± 3.0 mV, n = 5 cell pairs, mean of means) and to study spike transmission in this specific neuronal circuit (**Fig. 1***A1*). Solitary presynaptic PC spikes (interval 10 s) triggered single action potentials in the postsynaptic FSBCs, and the FSBC firing was abolished by postsynaptic hyperpolarization in all cell pairs studied (to -73.3 ± 5.2 mV, n = 5 cell pairs, mean of means) indicating that the spikes were triggered by the VLEs (see **Fig. 1***A2*). The postsynaptic interneurons exhibited narrow spike width (half-width 0.32 ± 0.05 ms, n = 5 cells, mean of means) and little firing frequency accommodation

during a suprathreshold depolarizing step (see **Fig. 1***A3*) (Szegedi et al., 2016; Wang et al., 2016). The interneurons were filled with biocytin and they showed axon forming boutons around L2-3 cell somata (see **Fig. 1***A3-4*) (Molnar et al., 2008; Blazquez-Llorca et al., 2010). One cell was tested for parvalbumin (pv) and found to be immunopositive (see **Fig. 1***A4*). The FSBCs were recorded in tissue material resected from frontal or temporal lobe as reported in detail in **Table 1**.

The master PC spike (interval 10 s) -evoked action potential in the FSBCs (Vm = -61.2 ± 3.2 mV, n = 5 cells, mean of means) showed short (2.67 ms average) delay (n = 117 spikes in 150 cycles of 5 cell pairs, 30 cycles in each) relative to the PC spike with 0.78 ± 0.10 probability (**Fig. 1***B-F*). The evoked firing in the five FSBCs (FSBC 1-5), the VLE amplitudes that failed to trigger the spike, and the firing threshold for 30 consecutive PC spike cycles are shown in **Fig. 1***B1-4* (FSBC 1) and **Fig.1***C1-F1* (FSBC 2-5). The FSBC firing delay results are depicted in raster plots and summarized with histograms in **Fig. 1***B5* (FSBC 1) and **Fig. 1***C2-F2* (FSBC 2-5).

The VLEs were stabile over the consecutive cycles of PC spikes (30 cycles) and showed 1.56 ± 0.27 ms time-to-peak (n = 5 cells, mean of means) and the maximum rise slope of 32.46 ± 1.12 mV/ms (n = 150 events in 5 cells) with small trial-to-trial variation of the slope (cv slope = 0.15 ± 0.02, n = 5 cells). The VLE rise-slope values and their stability for the 30 consecutive cycles in the FSBCs are illustrated in **Fig. 1***B6* (FSBC 1) and **Fig. 1***C3-F3* (FSBC 2-5).

In order to investigate whether the master PC -evoked firing varies between different type of interneurons, we recorded from three cell pairs where a master PC elicited firing in a non-fast spiking interneuron (non-FSIN) through VLEs (see **Fig. 2***A1-3,* **Table 1**). Unlike the FSBCs, these interneurons had slow spike kinetics (spike half-width 0.51±

0.06 ms, n = 3 cells, mean of means) (DeFelipe et al., 2013; Szegedi et al., 2016). The VLEs (interval 10 s) evoked maximally single action potential (Vm = -56.2 ± 5.4 mV, n = 3, mean of means) with 6.35 ms average delay to the PC spike (43 spikes in 82 cycles, in 3 cells) at 0.58 ± 0.22 probability (n = 3). Panels **Fig. 2***A4* (non-FSIN 1), The results are illustrated in figure 2 as follows: **Fig. 2***B1* (non-FSIN 2) and **Fig. 1***C1* (non-FSIN 3) illustrate the VLE-evoked firing, the amplitude of VLEs failing to trigger the spike, and the firing threshold for the three non-FSINs in the consecutive cycles (30 cycles in non-FSIN1 and 2, 22 cycles in non-FSIN3). The VLE-evoked firing delay is illustrated in raster plots and summarized with histograms in **Fig. 2** panels *A5* (non-FSIN 1) and *B2* and *C2* (non-FSIN 2 and 3, respectively). Although the average VLE amplitude in the non-FSINs (9.7 ± 0.9 mV, n = 3 cells, mean of means) was not different from the VLEs observed in the FSBCs (P = 0.39, MW-test), the VLEs in non-FSINs had slower time-to-peak (5.78 ± 0.61 ms, n = 3 cells, mean of means, P = 0.038, MW-test) and lower maximum rise slope (9.28 ± 1.01 mV/ms, n = 82 events) than in the FSBCs (P = 0.001, n = 150 and 82 events, respectively, MW-test). In addition, the VLE rise slope trial-to-trial variation was larger in these cells (cv slope = 0.33 ± 0.06, n = 3) than in the FSBCs (P = 0.036, MW-test). The VLE rise slope values for the consecutive cycles are depicted for the non-FSINs in **Fig. 2** panels *A6* (non-FSIN 1) and *B3* and *C3* (non-FSIN 2 and 3, respectively). Each non-FSIN showed prominent firing frequency accommodation or generated just single spike to a sustained depolarizing step as illustrated in **Fig. 2** panels *A7* (non-FSIN 1) and *B4* and *C4* (non-FSIN 2 and 3, respectively). The cells were filled with biocytin and visualized, and they showed multipolar somatodendritic structure with dendrites lacking spines. Reconstructions of the three PC to non-FSIN pairs are illustrated in **Fig. 2** panels *A8* (non-FSIN 1), *B5* and *C5* (non-FSIN 2 and 3).

Next, we compared the VLE-evoked spike delay between the FSBCs and the non-FSINs. In the FSBCs, the median spike delay varied between the cells from 1.61 ms (FSBC 5) to 5.0 ms (FSBC 2), and in the non-FSINs from 3.73 ms (non-FSIN1) to 14.7 ms (non-FSIN3). Altogether, the FSBCs showed shorter spike delay (median and interquartile range: FSBCs = 1.96, 1.68 to 3.25, non-FSINs = 5.60, 3.35 to 7.70, n = 117 and 43 spikes, respectively) and smaller spike delay variance than the non-FSINs (P = 0.001, MW-test). The FSBCs had membrane time constant of 8.6 ± 0.8 ms (n = 5) and the non-FSINs 7.2 ± 4.2 ms (n = 3). The spike delay values in the two cell groups are shown in detail in **Fig. 2***D1* with individual neurons' delay median, interquartile range, 5 and 95 percentiles, and the minimum and the maximum values (**Fig. 2***D2*), and statistical comparison of all spike delay values between the FSBCs and the non-FSIN1-2. (The non-FSIN3 was omitted in the analysis because of clearly lower number of spikes in the experiment compared to others).

Thus, in the human neocortex layer 2-3 fast-spiking basket cells show high fidelity "fast in - fast out" spike transmission (Hu et al., 2014) triggered by solitary master PC spikes. In addition, the master PC -triggered firing precision varies between layer 2-3 interneurons types, and the high precision discharge of the FSBCs is not seen in all interneuron types.

GABAergic interneuron discharge in the complex events is time-locked to master PC spike with a short interneuron-specific delay

Next, we examined discharge of GABAergic interneurons in complex events whilst avoiding direct microelectrode recording from the cells (Komlosi et al., 2012), since it

can potentially alter their excitability and the firing response to VLEs. We measured master PC spike -evoked inhibitory postsynaptic potentials (IPSPs) in L2-3 PCs. We analyzed the onset delay to the PC spike of 357 IPSPs (in 50 ms time window after a PC spike evoked every 10 s) recorded in 9 PC-PC pairs (269 cycles, 15-49 cycles per pair) most of them in the frontal or temporal cortex (see **Table 1**). The occurrence of IPSPs during the complex events in the experiments is summarized in **Fig. 3***A,B*. The majority of the IPSPs (n = 281 IPSPs) occurred during the first 10 ms of the complex events. These IPSPs were generated with high probability (0.87 ± 0.03 for the occurrence of IPSP in first 10 ms, n = 281 cycles in 9 cell pairs). In six experiments the predominant IPSP onset delay was < 5 ms (3.8 ± 0.2 ms, in 185 cycles in 6 pairs). In 3 experiments the main delay was longer and between 5 and 10 ms (7.9 ± 0.3 ms, n = 65 IPSPs in 96 cycles in 3 pairs, MW-test) (IPSP probability in first 10 ms 0.85 ± 0.02) (**Fig. 3***B*). In addition, various complex event episodes exhibited two or more IPSPs with distinct delays, with the later IPSPs showing lower probability than the first one (**Fig. 3***A,B*). Because in the experiments in figure 1 we had found that the master PCs elicited only single action potential in the GABAergic cells, we hypothesized that the occurrence of two or more IPSPs in same complex event episodes might emerge from separate GABAergic cells. Accordingly, we performed an experiment recording master PC -evoked IPSPs in two postsynaptic PCs simultaneously, but showing statistically different delays (3.72 ± 0.27 ms and 8.34 ± 0.23 ms, n = 8 and 6 IPSPs evoked in 14 cycles) (P = 0.002, t-test) and failures independent of each other (**Fig. 3***C*). The results indicate that the IPSPs emerged from the firing of distinct individual interneurons. Altogether, the results on the IPSPs in the PC-PC pairs demonstrate that master PC spikes trigger high fidelity discharge of some GABAergic interneurons with short and specific delay.

GABAergic synaptic currents with distinct kinetics manifest the activation of different interneuron subpopulations in complex events

Finally, we studied if the GABAergic synaptic activity during the master PC-evoked complex events would reflect the VLE-evoked discharge of the FSBCs as demonstrated in figure 1. As above, the experiments were performed in tissue samples mostly from the frontal or the temporal cortices (see **Table 1**). First, to investigate kinetic properties of distinct GABAergic neuron type -evoked IPSCs, we recorded from 15 monosynaptic interneuron to PC pairs in voltage clamp (at – 55 mV). In the connections from fast-spiking interneurons (FSINs, inward axon current width 0.45 ± 0.02 ms) to PCs, the IPSCs were 27.6 ± 2.2 pA in amplitude with 33.0 ± 1.9 pA/ms rise slope (n = 10 cell pairs, mean of means). Six of the successfully visualized FSINs were tested for parvalbumin (pv) and the vesicular GABA transporter (vgat) and found to be immunopositive for both (**Fig. 4***A1*). The six FSINs were identified as basket cells. In turn, monosynaptic IPSCs (average amplitude 22.0 ± 3.3 pA, n = 5) from non-FSINs (inward axon current width 0.93 ± 0.06 ms, n = 5 cells, mean of means, P = 0.003 compared to the FSINs, t-test) to PCs showed wide range of IPSC rise slope values in the studied pairs. In two non-FSIN connections to PC, the IPSCs were indistinguishable from those evoked by the FSINs (**Fig. 4***A2*), and in three connections the IPSCs showed distinctly slower rise slope (6.2 ± 3.8 pA/ms, n = 3, mean of means) than generated by any of the FSINs ($P < 0.05$ for each non-FSIN, Anova on ranks, Dunn's pairwise *post hoc* test with at least 5 events in each tested pair). The slope values in each recording were normalized by the IPSC amplitude in order to exclude any variation in the rise slopes possibly emerging from small differences in the IPSC electrochemical driving force

between individual experiments. The normalized rise slope of the FSIN-evoked currents was 1.25 ± 0.11 (n = 10 pairs, mean of means). The IPSCs from the non-FSINs had significantly slower normalized rise slope of 0.27 ± 0.10 (n = 3 pairs, mean of means) ($P < 0.05$ for each non-FSIN in Anova on ranks and Dunn's pairwise *post hoc* test against the FSINs with at least 5 events in each tested pair). The amplitude-normalized IPSC slope values for all cells are shown in **Fig. 4***A2*.

As the amplitude-normalized IPSC rise slope provides a robust tool to discriminate the fast IPSCs generated by FSBCs (and some non-FSINs) and the slow IPSCs emerging exclusively from non-FSINs, we investigated the IPSC rise slope in network activity episodes evoked by master PC single spikes (10 s interval) (**Fig. 4***B1-3*). The IPSCs in complex events had 24.4 ± 2.4 pA average amplitude (mean of means in 6 experiments), akin to the monosynaptic IPSCs in the 15 cell pairs studied above ($P = 0.91$, MW-test). We categorized complex event IPSCs by the amplitude-normalized rise slope value as shown by the monosynaptic IPSCs: the ratio > 0.7 similar to the IPSCs monosynaptically evoked by FSBCs as illustrated red in **Fig. 4***A2*, the ratio < 0.5 corresponding to IPSCs exclusively evoked by non-FSINs (illustrated green in **Fig. 4***A2*), and ratio 0.5 - 0.7 falling in between the two as defined in **Fig. 4***A2*. The occurrence of IPSCs and their rise slope (normalized by the amplitude) were analyzed in the complex events of six experiments as illustrated with sample traces in **Fig. 4***B1-3*.

We found that in four experiments the network-driven IPSCs with mainly fast amplitude-normalized rise slope (1.05 ± 0.10 average of all IPSCs in first 10 ms of complex events, n = 117 IPSCs in 172 complex events in 4 cells) predominated activity (**Fig. 4***C1-4*). When we focused the analysis on the first 10 ms (corresponding to monosynaptic spike time window observed in the FSBCs earlier), the fast rise time (>

410 0.7) IPSCs occurred in 84 cycles of the 172 cycles and showed 3.94 ms delay (median
411 with 3.55 to 5.20 ms interquartile range). The slow kinetic IPSCs (< 0.5) occurred only
412 in two experiments (**Fig. 4** panels *C2* and *C4*) with low probability (9 events in 172
413 cycles) in the same time window.

414 However, we found that in two experiments mostly slow kinetic IPSCs were generated,
415 although with low probability in the first 10 ms time window (14 in 122 cycles) and
416 only very few fast kinetic IPSCs events (4 in 122 cycles) occurred in the early (first 10
417 ms) of the events (**Fig. 4***D1-2*).

418 In order to compare the temporal distribution and the probability of the two types of
419 IPSCs (the fast and the slow) in the early complex events, we pooled the IPSCs in all 294
420 cycles of the 6 experiments. The results are illustrated in **Fig. 4***E* showing no difference
421 between the delay (P = 0.095, MW-test) of the fast IPSCs (median and interquartile
422 range: 4.08 ms, 3.56 to 5.30 ms) and the slow IPSCs (4.78 ms, 4.01 to 6.10 ms), but
423 demonstrating higher probability (P = 0.042, t-test) of occurrence of the fast than the
424 slow IPSCs in the early (first 10 ms) complex events.

425 In conclusion, the results demonstrate that IPSCs akin to those generated by FSBCs
426 regularly occur with a short delay and high temporal fidelity in the beginning of the
427 complex events in the experimental conditions that avoid direct recording from
428 interneurons. In addition, the experiments show that discharge of many non-FSINs
429 occurs at low probability.

430

431 DISCUSSION

Strong VLE-synapses from some layer 2-3 pyramidal cells to GABAergic interneurons represent a distinctive microcircuit feature in the human neocortex allowing these ”master PCs” to initiate tens-of-millisecond -long discharge in the local neuronal network by single action potentials (Molnar et al., 2008; Brecht, 2012; Lourenco and Bacci, 2017). Here we show that fast-spiking GABAergic basket cells are regularly activated at the beginning of these events with short delay and high temporal precision.

Microcircuits generating the complex events apparently represent a common feature in the human neocortex. The VLEs occur in about 10-15 % of the PC to FSIN synapses and the single PC spike-evoked interneuron firing has been reported in various neocortical areas in tissue samples resected from human subjects varying in age and gender (Molnar et al., 2008; Komlosi et al., 2012; Molnar et al., 2016). Although the specific function of the complex events, as characterized in the brain slices, is still unknown, the VLE-evoked accurate discharge of the fast-spiking basket cells and the disynaptic inhibition transferred from these interneurons could contribute to generation of co-ordinated network oscillations where FSBCs play a key role (Cunningham et al., 2004; Hajos et al., 2004; Ellender and Paulsen, 2010; Florez et al., 2015; Averkin et al., 2016). Importantly, unlike rodents the human neocortical microcircuits can trigger basket cell firing by a single master pyramidal cell action potential, and this may provide an important computational feature in cortical processing in the human compared to rodents (Lourenco and Bacci, 2017).

The temporal fidelity of the synaptically-triggered basket cell firing and the fast kinetic time-locked IPSCs in the early complex events reflect basket cells fast-in-fast-out signalling feature akin to characterized in these interneurons in rodents (Hu et al., 2014). The VLEs in the basket cells showed short time-to-peak value and a remarkably

fast rise slope, which together with their short membrane time constant can explain the short delay of the synaptically evoked spikes. The VLE synapses to fast-spiking interneurons have high release probability (Molnar et al., 2016), and this feature is in line with the observation here that the VLE rise slope value showed little variation in consecutive cycles in the FSBCs. This further increases temporal precision of the VLE-evoked spikes and explains their small jitter. In addition, the remarkably narrow time window of the VLE-evoked basket cell firing and the observation that only single spikes were generated by each VLE, may be set by autaptic GABAergic inhibitory synapses or GABAergic connections from other interneurons to these cells (Tamas et al., 1997; Hioki et al., 2013; Deleuze et al., 2014; Lourenco et al., 2014). Curiously, although one FSBC (FSBC 2) showed slightly longer average spike delay than the other basket cells investigated here, it along with the others also showed small spike delay jitter. The master PC -evoked firing of the non-FSINs showed lower temporal fidelity than the basket cells. This can be partly explained by the large trial-to-trial variation of the VLEs and the long VLE time-to-peak in the non-FSINs. Postsynaptic membrane potential and the VLE amplitude also regulate spike transmission (Kretzberg et al., 2001). Therefore, it is likely that these interneurons' input-output transformation is further controlled by brain state-dependent membrane potential fluctuations (Puig et al., 2008; Fanselow and Connors, 2010) and by plasticity of the VLEs (Szegedi et al., 2016).

Although this study almost entirely focuses on the fast-spiking basket cells, it also shows that in addition other cortical interneuron types discharge in complex events. In particular, we demonstrated the discharge of non-FSINs with variable delay and low probability (Szegedi et al., 2016). However, the non-FSINs in general comprise a highly diverse group of interneuron types and a separate study will be needed in the future to

investigate the firing behaviour of identified non-FSIN cell types (Tremblay et al., 2016). In addition, fast-spiking axo-axonic cells fire with a short delay akin to the FSBCs reported here and these GABAergic cells can excite pyramidal cells and may trigger their firing though depolarising GABAergic effect on the axon initial segment (Szabadics et al., 2006; Molnar et al., 2008; Komlosi et al., 2012). In line with this, polysynaptic EPSCs are often generated in complex events with 5 to 10 ms delay to a master PC spike, apparently evoked by these interneurons (Molnar et al., 2008; Komlosi et al., 2012) since VLE-like synaptic contacts have not been found between L2-3 PCs (Molnar et al., 2008; Szegedi et al., 2016).

In a slice preparation the complex event activity patterns can be deformed with partially pruned synaptic networks. This might explain why the fast- and the slow-kinetic IPSC occurrences showed very different patterns between some individual experiments here. Another more exciting possibility for this observation is that the distinct complex event structures genuinely reflect diversity of neuronal ensembles established in the brain prior to the resection of the cortical tissue. Although the hypothesis is challenging to address experimentally in humans, further investigation of distinct interneuron types discharge during the complex events will help to judge this idea.

To conclude, the results hitherto show that human cortical microcircuits generating complex events involve various specialized GABAergic interneuron types. We suggest that various cell types may show specific firing behaviour during the events as we report here for the FSBCs (Klausberger and Somogyi, 2008). Therefore the activation of FSBCs in early phase of the complex events may just represent one common feature in these human neocortex network activity episodes.

504

505 FIGURE AND TABLE LEGENDS

506 **Table 1.** Details showing the patient gender, age and the resected cortical area of the
507 tissue samples used in the experiments of this study. Cell ID refers to the cell pair code
508 used in the text and in the figures. Second column identifies the figure in which the
509 specific experiment data are illustrated. Experiment code refers to original
510 identification number of the cell pair in the authors' files, and last column shows patient
511 pathology diagnosed for the surgery.

512 **Figure 1.** Very large monosynaptic EPSP from single pyramidal cell triggers short-delay
513 high-precision discharge of fast-spiking basket cells.

514 ***A-B***, Solitary master pyramidal cell (PC, red) spikes trigger firing in a postsynaptic fast-
515 spiking basket cell (FSBC, blue) with a short delay and high temporal fidelity through
516 very large monosynaptic EPSP (VLEs). (*A1*) Single PC spikes (elicited with 2-3 ms
517 suprathreshold depolarizing pulses) trigger discharge in fast-spiking basket cell 1 (FSBC
518 1, Vm = –61 mV) with occasional failures (6 consecutive responses superimposed).
519 Schematic summarizes experimental design. (*A2*) FSBC 1 hyperpolarization precludes
520 the action potential revealing monosynaptic VLE (blue, 6 consecutive responses
521 superimposed). (*A3*) Illustration of the PC (soma and dendrites red, axon orange) to
522 FSBC 1 (blue, axon light blue) -pair with VLEs. L1 and L2-3 = layer 1 and 2-3,
523 respectively. Scale 100 µm. Inset below shows the FSBC 1 firing response without
524 apparent firing accommodation (600 ms depolarizing pulse). Scales 60 mV, 100 ms.
525 (*A4*) Biocytin-filled postsynaptic FSBC (FSBC 2) axon in L2-3. *Left:* Axon boutons
526 (indicated by arrows) are arranged around an unlabelled L2-3 cell soma (asterisk,

endofluorescence in nucleus). *Right*: biocytin (Cy3) -filled bouton with positive immunoreaction (arrow) for pv (Alexa488) and vgat (Cy5) in the same cell. Scale 5 μm. (*B1*) Average of the VLEs that failed to fire (6) in the FSBC 1. (*B2*) Consecutive VLEs each eliciting single action potential in the FSBC 1 (blue, 6 events including a VLE that failed to fire) by solitary PC spikes (10 s interval, one sample shown in red). (*B3*) Derivative (black line) of a VLE with spike (blue line). Arrow indicates the VLE maximum rise slope, and the following hump in the derivative corresponds to the action potential onset. The onset membrane potential (Vm) is indicated by horizontal dotted red line. (*B4*) Firing of the FSBC 1 by VLEs for 30 consecutive PC spikes (10 s interval). Open circles show the FSBC 1 membrane potential (Vm). Red marks show Vm for the onset of the triggered action potentials. Green bars illustrate the amplitude of the VLEs that failed to fire. (*B5*) Timing of the FSBC 1 firing (black dots) in the 30 consecutive cycles. Blue histogram summarizes the evoked spike delay distribution (count, bin 0.25 ms). (*B6*) The VLE maximum rise slope plotted for the 30 consecutive responses (as in *B2* and *B4*).

C-F, High temporal fidelity characterizes spike transmission in PC-FSBC pairs connected with VLEs. Experiments as in A-B in four PC-FSBC pairs (FSBC 2-5) showing VLEs. (*C1*) FSBC 2 membrane potential (Vm) in 30 consecutive cycles of PC spike. Red marks, membrane potential (Vm) for the onset of the postsynaptic action potentials. Green bars show amplitude of the VLEs that failed to fire. (*C2*) Timing of the FSBC 2 firing (black dots) in the 30 cycles. Histogram (blue, bin 0.25 ms) summarizes the spike delay distribution. *Inset:* Two sample traces in the experiment showing a VLE triggering (blue) and failing to trigger (green) an action potential. Scale 10 mV, 30 ms. The spike amplitude is truncated. (*C3*) The VLE maximum rise slope in the 30 consecutive

551 responses. (*D1-D3*, *E1-E3*, *F1-F3*) Data show similar experiments for three other PC to
552 FSBC (FSBC 3-5) pairs. *Insets:* Scaling as above, action potential amplitudes are
553 truncated. Note that in the FSBC 3 and FSBC 5 the large VLEs at relatively negative
554 postsynaptic Vm partially mask spike afterhyperpolarization.

555

556 **Figure 2.** A pyramidal cell spike triggers firing in non-fast spiking interneurons with
557 short delay but low temporal fidelity.

558 ***A-C***, Three paired recordings showing PCs connected monosynaptically to non-fast
559 spiking interneurons (non-FSINs) though VLEs that trigger their firing. ***A***, A PC
560 connected to non-FSIN 1. (*A1*) Average of VLEs (3) that failed to fire. (*A2*) VLEs with
561 action potential in 5 events (blue) triggered by solitary PC spikes (10 s interval, a
562 sample shown in red). Schematic shows the experimental design. (*A3*) Derivative (black
563 line) of a VLE with action potential (blue line). Arrow shows the VLE maximum rise
564 slope, and the following hump in the black line marks the action potential onset. The
565 onset membrane potential in the blue line is indicated by horizontal dotted red line.
566 (*A4*) Firing evoked by the VLEs for 30 consecutive PC spikes (10 s interval). Open circles
567 indicate the interneuron membrane potential (Vm), red marks show Vm for the
568 triggered action potential onsets. Green bars show amplitude of the VLEs that failed to
569 trigger firing. (*A5*) Timing of the non-FSIN 1 firing (black dots) in the 30 cycles. Blue
570 histogram summarizes the evoked spike delay (count, bin 0.25 ms). (*A6*) The VLE
571 maximum rise slope shows large trial-to-trial variability (30 consecutive cycles)
572 including EPSP failure in cycle 15. (*A7*) The non-FSIN 1 firing response to a sustained
573 depolarizing (600 ms) step shows clear firing frequency accommodation. Scale 60 mV,
574 100 ms. (*A8*) Illustration of the presynaptic PC (soma and dendrites red, axon orange)

and the postsynaptic non-FSIN 1 (blue, axon light blue). L1 and L2-3 = layer 1 and 2-3, respectively. Scale 100 µm. ***B***, Similar analyses of another PC to non-fast spiking interneuron (non-FSIN 2) pair with VLEs. (*B1*) The non-FSIN 2 membrane potential (Vm, open circles) in 30 consecutive cycles of PC spikes (10 s interval). Red marks show Vm for onsets of the postsynaptic action potentials. Green bars illustrate amplitude of the VLEs that failed to fire. (*B2*) Timing of the firing (black dots) in the 30 cycles. Histogram (bin 0.25 ms) summarizes the spike delay distribution. (*B3*) The VLE maximum rise slope in the consecutive cycles. Note large trial-to-trial variability. (*B4*) The non-FSIN 2 shows just single action potential for a (600 ms) depolarizing pulse. Scale 60 mV, 100 ms. (*B5*) Illustration of the PC (soma and dendrites red, axon orange) and the postsynaptic non-FSIN 2 (blue, axon light blue). L1 and L2-3 = layer 1 and 2-3, respectively. Scale 100 µm. ***C***, Analyses of a PC to non-FSIN 3 pair with VLEs. (*C1*) The Vm (open circles), the membrane potential for the action potential onset (red marks), and the amplitude of VLEs that failed to fire (green bars) in consecutive (22) cycles. (*C2*) Timing of the firing (black dots) and a histogram (bin 0.25 ms) summarizing the postsynaptic spike delay. (*C3*) The VLE maximum rise slope for the cycles shows again notable trial-to-trial variability. (*C4*) The interneuron firing shows clear firing frequency accommodation to a sustained depolarizing pulse. Scale 60 mV, 100 ms. (*C5*) Illustration of the cell pair. ***D***, The FSBCs show shorter average spike delay and smaller spike delay variance than the non-FSINs. (*D1*) Cumulative histograms showing the VLE-evoked spike delays in the FSBC 1-5 and in the non-FSIN 1 and the non-FSIN 2. Spike delay data from the non-FSIN 3 was omitted here, because the experiment showed only four data points and most of them with longer than 10 ms delay. (*D2*) The spike delay values in the cells showing each individual neuron delay median, interquartile range, 5 and 95 percentiles and the minimum and maximum values. Mann-Whitney test shows

600 significant difference between the spike delay values of the FSBCs and of the non-FSIN
601 1-2. The non-FSIN 3 is omitted in the test because of the very low number of evoked
602 spikes compared to the other cells.

603

604 **Figure 3.** A pyramidal cell spike triggers GABAergic synaptic events with short delay
605 and high temporal precision**.**

606 ***A***, Simultaneous recording from two pyramidal cells demonstrates that solitary PC
607 spikes elicit time-locked GABAergic IPSPs with a few millisecond onset delay. A sample
608 recording in the cell pair 1 shows single PC spike -evoked GABAergic IPSPs with two
609 predominant delays during first 10 ms of the triggered activity. The IPSPs with the
610 distinct delays occur successively in individual complex event episodes. *(A1)* a PC spike
611 and 10 consecutive complex event episodes showing IPSPs (at – 55 mV). *(A2)* plot
612 shows timing of the IPSPs. Dots indicate the IPSP onset delay to the PC spike in
613 consecutive cycles (49 cycles, PC spike interval 10 s). Schematic shows the experimental
614 design. Histogram summarizes the IPSP count against the IPSP onset delay (bin 1 ms).

615 ***B***, Line histograms show IPSP onset delays in eight similar PC-PC pair recordings (cell
616 pairs 2-9) as shown in *A*, illustrated here in different colors. Ordinates show the IPSP
617 count. From top down, the experiments first show complex event patterns with
618 occurrence of single delay peak (cell pairs 2-5), then complex pattern activity where the
619 short-delay peak is followed by IPSPs with longer delay and lower probability (cell pairs
620 6-7), and finally cell pairs (8-9) where the complex events are comprised of loosely
621 time-locked IPSPs occurring at low probability.

C, IPSPs are time-locked to PC spike with pathway-specific delays. Recording from a PC-PC pair (cell pair 10) shows two IPSPs time-locked to PC1 spike (interval 10 s) with average delay of 3.7 ms (in PC2) and 8.3 ms (in PC1). The IPSPs are generated by separate interneurons as revealed by cycles showing independent failures in either PC1 (green) or in PC2 (magenta).

Figure 4. GABAergic synaptic currents with fast- or slow rise slope reveal the discharge of different interneurons in the complex events.

A, GABAergic synaptic currents from FSBCs and some non-FSINs show different kinetic features in L2-3 pyramidal cells. (*A1*) One visualized synaptically connected FSBC (blue, axon light blue) to PC pair (red, axon orange). L1 and L2-3 indicate the layers 1 and 2-3, respectively. Scale 100 µm. *Insets*: Schematic summarizes the experimental design. Traces show four superimposed consecutive monosynaptic IPSCs in the postsynaptic PC (red traces, at – 55 mV) evoked by the FSBC spikes (black trace, interval 10 s). Micrographs illustrate pv+ (Alexa488) and vgat+ (Cy5) axon boutons of the biocytin-filled (Cy3) presynaptic FSBC. Scale 5 µm. (*A2*) Monosynaptic IPSCs evoked from FSBCs and some non-FSINs to PCs show distinct IPSC rise slope kinetics. *Top*: Sample monosynaptic IPSCs (4) in postsynaptic PCs (red traces, at – 55 mV) evoked by spikes (single traces shown in black) of a FSBC or a non-FSIN. *Bottom*: Plot shows monosynaptic IPSC rise slope kinetics (IPSC rise slope normalized by the amplitude) in 15 interneuron to PC pairs. The value variation in individual cells correlates inversely with the IPSC amplitude indicating it emerges from release asynchrony (see methods). Red dots show IPSCs from identified FSBCs. Green dots show slow IPSCs exclusively evoked from non-FSINs. pv+ BC, parvalbumin immunopositive fast-spiking basket cells;

uFS, fast-spiking cells not successfully visualized and identified; non-FS, non-fast spiking cells.

B-D, Recordings from PC-PC pairs show network-driven IPSCs with distinct rise slope kinetics in the complex events. (*B1*) A sample recording in voltage clamp (at –55 mV) showing the occurrence and the delay of a PC spike (10 s interval, 43 cycles) –evoked IPSCs (same experiment as the cell pair 3 below). (*B2*) Sample trace in one experiment showing a fast network-driven IPSC (red) defined by the high rise kinetics. The IPSC derivative is shown in grey. (*B3*) Sample trace showing an evoked slow kinetic IPSC (green) followed by a fast IPSC (red) in a complex event. (*C1-4*) PC spike-evoked complex events showing predominantly IPSCs akin to those generated by the FSBCs with fast rise-slope (red, rise slope to amplitude ratio > 0.7) in the beginning (during first 10 ms) of the events. Green dots indicate IPSCs with slow rise slope akin to those generated exclusively by the non-FSINs (ratio < 0.5). IPSCs with the amplitude-normalized rise slope value from 0.5 to 0.7 are indicated in brown. The plots show the IPSC amplitude-normalized rise slope value (ordinate) versus the IPSC delay (abscissa, 0 time point indicates timing of the master PC spike). The line histograms (bin 1 ms) below summarize the delay distribution of the fast (red, ratio > 0.7) and the slow (green, ratio < 0.5) IPSCs in each experiment (number of the cycles shown in parentheses). Line histogram ordinate shows count. The early complex event (first 10 ms) in the plots is marked with shaded background. (*D1-2*) Similar dot plots and histograms from two PC-PC pair recordings showing complex events with predominantly slow IPSCs (ratio < 0.5) and only occasional fast IPSCs.

E, *Top:* Summary of the onset delay values of the fast IPSCs (ratio > 0.7, red) and the slow IPSCs (ratio < 0.5, green) pooled in all 294 complex events in the six experiments

in early phase of the complex events (during first 10 ms). Box plot shows median, interquartile range, 5 and 95 percentiles and the minimum and maximum measured in the first 10 ms of the events. *Bottom:* Plot shows higher probability of the fast IPSCs (events/cycle) than the slow IPSCs in the six experiments (t-test). Individual dots show the probability in the individual experiments.

REFERENCES

Ainsworth M, Lee S, Cunningham MO, Traub RD, Kopell NJ, Whittington MA (2012) Rates and rhythms: a synergistic view of frequency and temporal coding in neuronal networks. *Neuron* **75**:572-583.

Averkin RG, Szemenyei V, Borde S, Tamas G (2016) Identified Cellular Correlates of Neocortical Ripple and High-Gamma Oscillations during Spindles of Natural Sleep. *Neuron* **92**:916-928.

Blazquez-Llorca L, Garcia-Marin V, DeFelipe J (2010) GABAergic complex basket formations in the human neocortex. *J Comp Neurol* **518**:4917-4937.

Brecht M (2012) Neuronal communication: firing spikes with spikes. *Curr Biol* **22**:R633-635.

Buzsaki G, Watson BO (2012) Brain rhythms and neural syntax: implications for efficient coding of cognitive content and neuropsychiatric disease. *Dial Clin Neurosci* **14**:345-367.

Cunningham MO, Halliday DM, Davies CH, Traub RD, Buhl EH, Whittington MA (2004) Coexistence of gamma and high-frequency oscillations in rat medial entorhinal cortex in vitro. *J Physiol* **559**:347-353.

693 DeFelipe J et al. (2013) New insights into the classification and nomenclature of cortical
694 GABAergic interneurons. *Nat Rev Neurosci* **14**:202-216.
695 Deleuze C, Pazienti A, Bacci A (2014) Autaptic self-inhibition of cortical GABAergic
696 neurons: synaptic narcissism or useful introspection? *Curr Opinion Neurobiol*
697 **26**:64-71.
698 Doron G, Brecht M (2015) What single-cell stimulation has told us about neural coding.
699 *Phil trans Royal Soc London Ser B, Biol sci* **370**:20140204.
700 Ellender TJ, Paulsen O (2010) The many tunes of perisomatic targeting interneurons in
701 the hippocampal network. *Front Cell Neurosci* **4**:00026.
702 Fanselow EE, Connors BW (2010) The roles of somatostatin-expressing (GIN) and fast-
703 spiking inhibitory interneurons in UP-DOWN states of mouse neocortex. *J*
704 *Neurophysiol* **104**:596-606.
705 Florez CM, McGinn RJ, Lukankin V, Marwa I, Sugumar S, Dian J, Hazrati LN, Carlen PL,
706 Zhang L, Valiante TA (2015) In vitro recordings of human neocortical
707 oscillations. *Cereb Cortex* **25**:578-597.
708 Hajos N, Palhalmi J, Mann EO, Nemeth B, Paulsen O, Freund TF (2004) Spike timing of
709 distinct types of GABAergic interneuron during hippocampal gamma oscillations
710 in vitro. *J Neurosci* **24**:9127-9137.
711 Hioki H, Okamoto S, Konno M, Kameda H, Sohn J, Kuramoto E, Fujiyama F, Kaneko T
712 (2013) Cell type-specific inhibitory inputs to dendritic and somatic
713 compartments of parvalbumin-expressing neocortical interneuron. *J Neurosci*
714 **33**:544-555.
715 Hu H, Gan J, Jonas P (2014) Interneurons. Fast-spiking, parvalbumin(+) GABAergic
716 interneurons: from cellular design to microcircuit function. *Science*
717 **345**:1255263.

718 Isaacson JS, Scanziani M (2011) How inhibition shapes cortical activity. *Neuron* **72**:231-
719 243.
720 Klausberger T, Somogyi P (2008) Neuronal diversity and temporal dynamics: the unity
721 of hippocampal circuit operations. *Science* **321**:53-57.
722 Komlosi G, Molnar G, Rozsa M, Olah S, Barzo P, Tamas G (2012) Fluoxetine (prozac) and
723 serotonin act on excitatory synaptic transmission to suppress single layer 2/3
724 pyramidal neuron-triggered cell assemblies in the human prefrontal cortex. *J*
725 *Neurosci* **32**:16369-16378.
726 Kretzberg J, Egelhaaf M, Warzecha AK (2001) Membrane potential fluctuations
727 determine the precision of spike timing and synchronous activity: a model study.
728 *J Comput Neurosci* **10**:79-97.
729 Lewis DA, Curley AA, Glausier JR, Volk DW (2012) Cortical parvalbumin interneurons
730 and cognitive dysfunction in schizophrenia. *Trends Neurosci* **35**:57-67.
731 Lourenco J, Bacci A (2017) Human-Specific Cortical Synaptic Connections and Their
732 Plasticity: Is That What Makes Us Human? *PLoS Biol* **15**:e2001378.
733 Lourenco J, Pacioni S, Rebola N, van Woerden GM, Marinelli S, DiGregorio D, Bacci A
734 (2014) Non-associative potentiation of perisomatic inhibition alters the
735 temporal coding of neocortical layer 5 pyramidal neurons. *PLoS Biol*
736 **12**:e1001903.
737 Mody I, De Koninck Y, Otis TS, Soltesz I (1994) Bridging the cleft at GABA synapses in
738 the brain. *Trends Neurosci* **17**:517-525.
739 Molnar G, Rozsa M, Baka J, Holderith N, Barzo P, Nusser Z, Tamas G (2016) Human
740 pyramidal to interneuron synapses are mediated by multi-vesicular release and
741 multiple docked vesicles. *eLife* **18167**.

742 Molnar G, Olah S, Komlosi G, Fule M, Szabadics J, Varga C, Barzo P, Tamas G (2008)
743 Complex events initiated by individual spikes in the human cerebral cortex. *PLoS*
744 *Biol* **6**:e222.
745 Puig MV, Ushimaru M, Kawaguchi Y (2008) Two distinct activity patterns of fast-spiking
746 interneurons during neocortical UP states. *Proc Natl Acad Sci U S A* **105**:8428-
747 8433.
748 Szabadics J, Varga C, Molnar G, Olah S, Barzo P, Tamas G (2006) Excitatory effect of
749 GABAergic axo-axonic cells in cortical microcircuits. *Science* **311**:233-235.
750 Szegedi V, Paizs M, Csakvari E, Molnar G, Barzo P, Tamas G, Lamsa K (2016) Plasticity in
751 Single Axon Glutamatergic Connection to GABAergic Interneurons Regulates
752 Complex Events in the Human Neocortex. *PLoS Biol* **14**:e2000237.
753 Tamas G, Buhl EH, Somogyi P (1997) Massive autaptic self-innervation of GABAergic
754 neurons in cat visual cortex. *J Neurosci* **17**:6352-6364.
755 Tremblay R, Lee S, Rudy B (2016) GABAergic Interneurons in the Neocortex: From
756 Cellular Properties to Circuits. *Neuron* **91**:260-292.
757 Wang B, Ke W, Guang J, Chen G, Yin L, Deng S, He Q, Liu Y, He T, Zheng R, Jiang Y, Zhang
758 X, Li T, Luan G, Lu HD, Zhang M, Shu Y (2016) Firing Frequency Maxima of Fast-
759 Spiking Neurons in Human, Monkey, and Mouse Neocortex. *Front Cell Neurosci*
760 **10**:239.

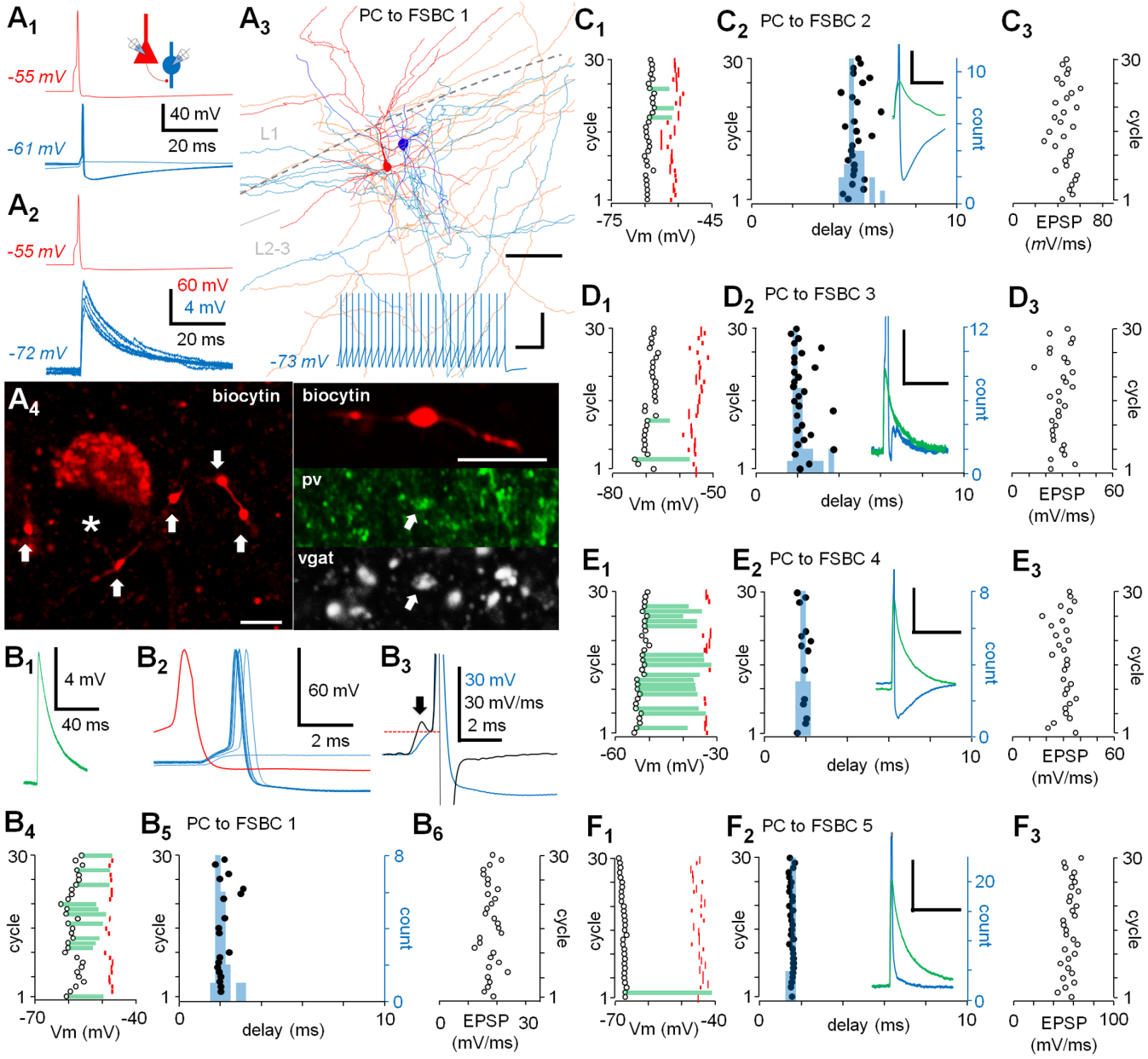

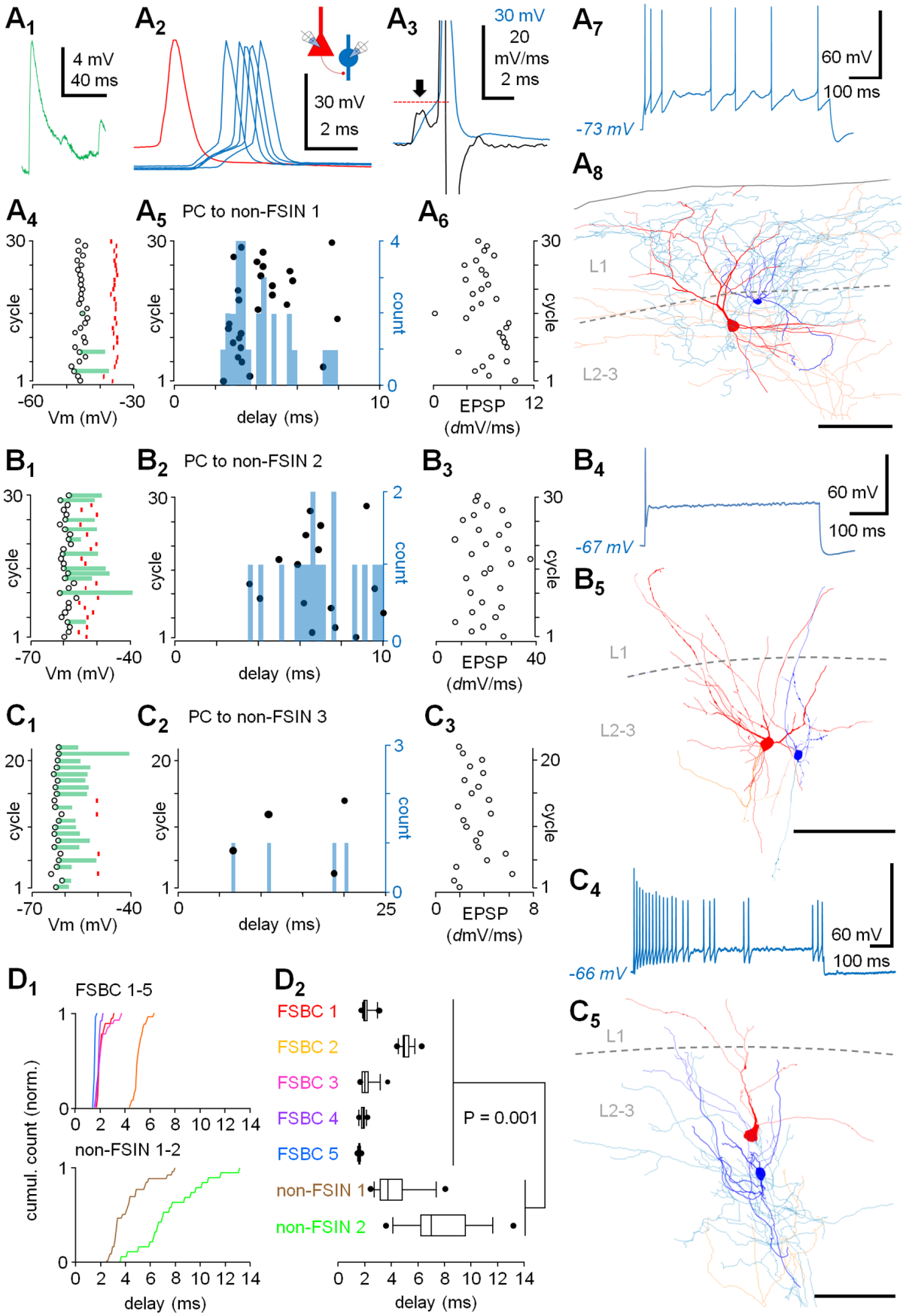

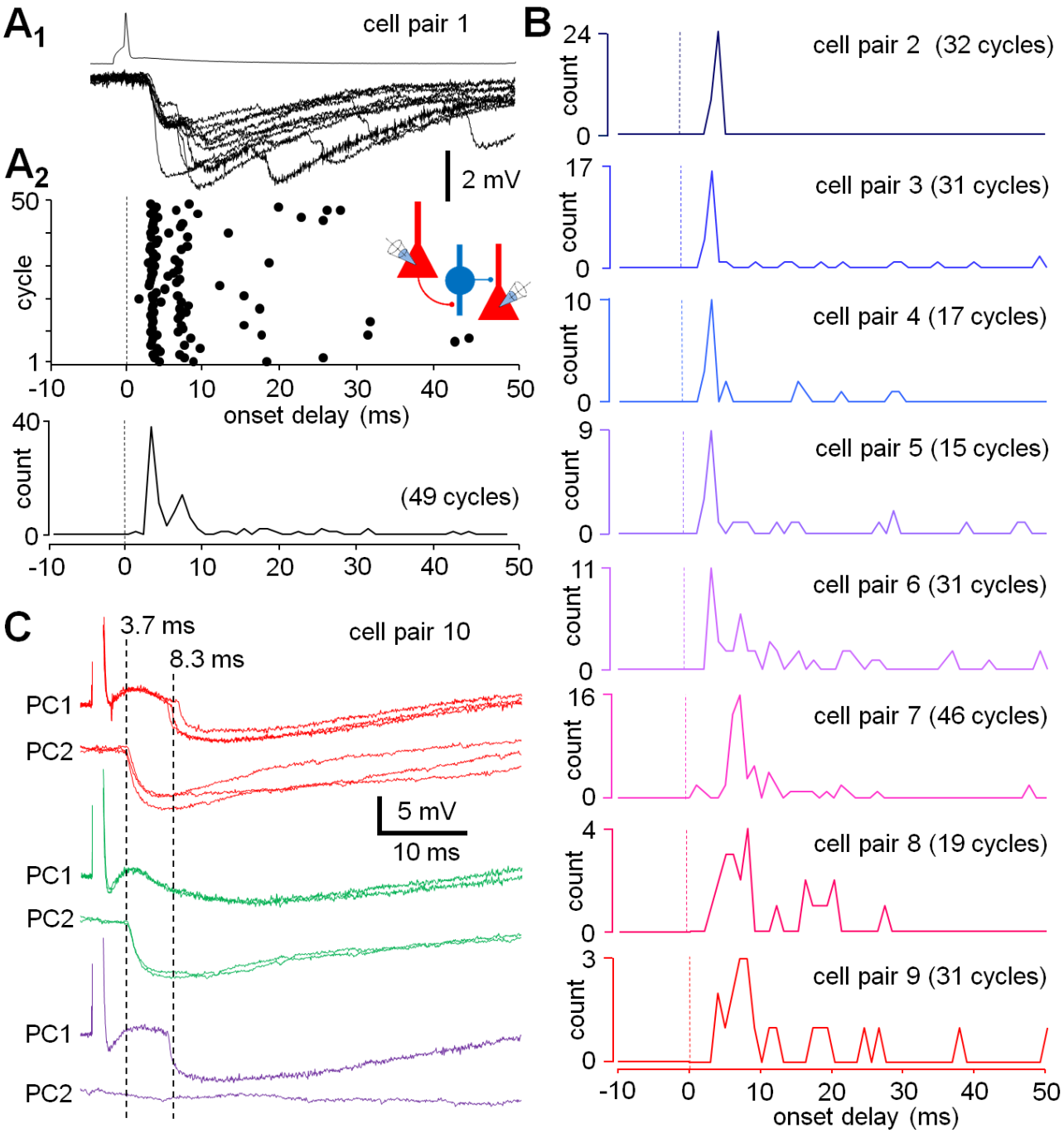

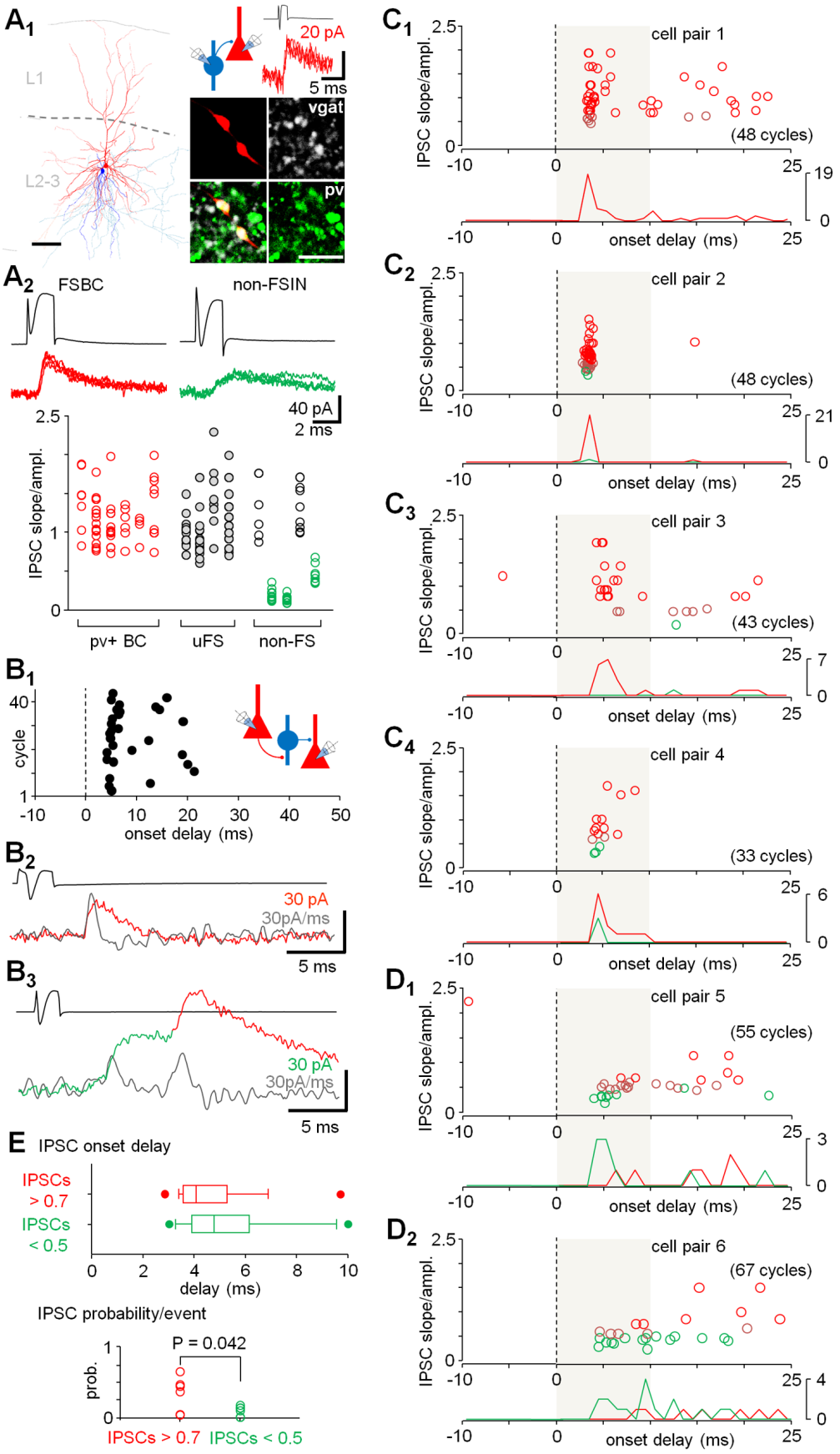

Cell ID	Figure showing the data	Gender	Age (years)	Hemisphere	Neocortical area (material removed to gain access to surgical treatment of pathological targets)	Experiment code	Diagnosed pathology
FSBC 1	Fig. 1A,B	male	49	left	temporal	0501043j	Cortical and subcortical neoplasm
FSBC 2	Fig. 1C	female	42	left	frontal	K1901171	Subcortical neoplasm
FSBC 3	Fig. 1D	male	43	left	temporal	1403062	Subcortical neoplasm
FSBC 4	Fig. 1E	male	29	right	frontal	0609121s	Cortical and subcortical neoplasm
FSBC 5	Fig. 1F	male	54	right	temporal	0705173s	Cortical and subcortical neoplasm
non-FSIN 1	Fig. 2A	male	58	right	temporal	0512022	Subcortical neoplasm
non-FSIN 2	Fig. 2B	female	68	right	temporoparietal	k0205171	Cortical and subcortical metaplasia
non-FSIN 3	Fig. 2C	female	64	right	frontal	0601171	Subcortical neoplasm
Cell pair 1	Fig. 3A	male	40	left	temporal	1405151	Subcortical neoplasm
Cell pair 2	Fig. 3B	male	58	left	temporal	1509122	Subcortical neoplasm
Cell pair 3	Fig. 3B	male	36	left	temporal	1311131	Subcortical neoplasm
Cell pair 4	Fig. 3B	male	17	left	parieto-occipital	1110271	Cortical and subcortical neoplasm
Cell pair 5	Fig. 3B	male	48	right	frontal	1401233	Subcortical aneurysm
Cell pair 6	Fig. 3B	male	40	left	temporal	1405152	Subcortical neoplasm
Cell pair 7	Fig. 3B	male	49	right	frontal	1310092	Meningioma
Cell pair 8	Fig. 3B	male	36	right	temporal	1112082	Subcortical neoplasm
Cell pair 9	Fig. 3B	male	16	right	parieto-occipital	1402181	Subcortical neoplasm
Cell pair 10	Fig. 3C	female	33	right	temporal	1510301	Cortical and subcortical neoplasm
pv+ BC 1	Fig. 4A	male	55	right	frontal	k0409152	Cortical and subcortical neoplasm
pv+ BC 2	Fig. 4A	female	10	left	frontal	k2506151	Subcortical neoplasm
pv+ BC 3	Fig. 4A	female	10	left	frontal	k2506155	Subcortical neoplasm
pv+ BC 4	Fig. 4A	female	30	left	parieto-occipital	k2306151	Shunt for hydrocephalus
pv+ BC 5	Fig. 4A	female	40	right	frontal	k2309153	Subcortical neoplasm
pv+ BC 6	Fig. 4A	female	28	right	parieto-occipital	k2804151	Subcortical neoplasm
uFS 1	Fig. 4A	female	67	right	frontal	100306c11	Epidural hemorrhage
uFS 2	Fig. 4A	male	55	right	frontal	040915c11	Cortical and subcortical neoplasm
uFS 3	Fig. 4A	male	47	right	frontal	021005c3	Cortical and subcortical metaplasia
uFS 4	Fig. 4A	female	59	right	frontal	K2510161	Shunt for hydrocephalus
non-FS 1	Fig. 4A	female	33	right	temporal	301015c1	Cortical and subcortical neoplasm
non-FS 2	Fig. 4A	male	19	right	parieto-occipital	151015c3	Shunt for hydrocephalus
non-FS 3	Fig. 4A	female	33	left	parieto-occipital	051115c7	Meningioma
non-FS 4	Fig. 4A	female	37	right	temporal	050416t6	Subcortical neoplasm
non-FS 5	Fig. 4A	male	47	right	frontal	021015c12	Subcortical neoplasm
Cell pair 1	Fig. 4C	female	55	left	frontal	k1208152	Shunt for hydrocephalus
Cell pair 2	Fig. 4C	male	58	left	temporal	k0109151	Subcortical neoplasm
Cell pair 3	Fig. 4C	female	50	right	frontal	k2511161	Subcortical neoplasm
Cell pair 4	Fig. 4C	female	33	left	parieto-occipital	k0511151	Meningioma
Cell pair 5	Fig. 4D	female	55	left	temporal	k1208151	Subcortical neoplasm
Cell pair 6	Fig. 4D	male	60	left	temporal	k2806161	Subcortical neoplasm